

Plasma-Assisted Production of Carbon Black and Carbon Nanotubes from Methane by Thermal Plasma Reform

Vanessa Z. Baldissarelli,* Luís Otávio de B. Benetoli, Felipe A. Cassini,
Ivan G. de Souza and Nito A. Debacher

Universidade Federal de Santa Catarina, Departamento de Química - CFM,
Campus Universitário Trindade, CP 476, 88040-900 Florianópolis-SC, Brazil

A reforma de fontes de carbono por plasma térmico de argônio de elevada capacidade calorífica é um dos métodos mais promissores na síntese de novos materiais. Um método para a obtenção de negro de carbono e nanotubos de carbono através da pirólise do metano por plasma térmico de corrente contínua é relatado no presente trabalho. A reforma foi realizada na ausência de oxigênio utilizando um jato de plasma gerado por uma tocha de plasma de argônio. O produto sólido foi caracterizado por espectroscopia Raman e microscopia eletrônica de varredura e transmissão. Os resultados mostraram que nanotubos de carbono foram produzidos na presença de catalisadores metálicos, enquanto que a formação de negro de carbono ocorreu na ausência de catalisadores no reator. A relação I_D/I_G obtida a partir dos espectros Raman indicou que a amostra obtida usando o catalisador 5%Ni/Al₂O₃ apresentou nanotubos de carbono com maior pureza em relação aos outros catalisadores (10%Ni/Al₂O₃ e 10%Ni-5%Ce/Al₂O₃) testados.

Thermal plasma processing of carbon sources using a plasma jet with high heat capacity is one of the most promising methods for the synthesis of new materials. A method for obtaining carbon black (CB) and carbon nanotubes (CNT) through the pyrolysis of methane using a thermal plasma direct current (DC) system is reported herein. The cracking operation is performed in the absence of oxygen using an external power source, i.e., a plasma jet generated by an argon plasma torch. The obtained carbonaceous materials were characterized by Raman spectroscopy, scanning, and transmission electron microscopy. The results showed that CNT are produced in the presence of a catalyst while CB formation occurs without a catalyst. The Raman I_D/I_G ratio indicated that the sample obtained using a 5%Ni/Al₂O₃ catalyst contains a higher quantity of pure CNT than the other catalysts tested (10%Ni/Al₂O₃ and 10%Ni-5%Ce/Al₂O₃).

Keywords: plasma processing, carbon nanotubes, carbon black, metal catalyst

Introduction

Recent indications of global warming caused primarily by the emission of greenhouse gases have drawn attention to the fact that the current industrial production methods are not compatible with sustainable development. Of all the gases that may contribute to the greenhouse effect, methane (CH₄) deserves special attention since the major sources of its emission are related to industrial processes. Successful research and development aimed at identifying a viable use for CH₄ is associated with the achievement of two main goals: mitigation of the accumulation of this

greenhouse gas in the atmosphere and improved efficiency in the use of carbon sources.

Conventional technologies based on, for instance, incineration, catalysis, adsorption and disposal in landfill have been extensively applied to the abatement of pollutant gases. Plasma technology has been demonstrated to be suitable for treating a large number of gaseous pollutants due to its many advantages in comparison to other technologies including non-selective treatment, higher energy efficiencies,¹ high energy density and temperatures, and fast reaction times.²

In the case of CH₄ gas treatment, the main products generated by the chemical reactions triggered by the thermal plasma source are hydrogen and a variety of carbon nanomaterials, including fullerenes,³ CNT⁴ and CB,⁵ all

*e-mail: vanessabaldissarelli@gmail.com

of which are of great economic interest. The allotropic forms of carbon of considerable interest in this study are CNT and CB.

According to Harbec *et al.*⁶ CNT are long hollow tubes containing hundreds of carbon atoms, and they are characterized by their nanometer diameter and their micrometer length, giving them a roughly one-dimensional structure. However, for their industrial application a continuous process of large-scale production is essential. Plasma-enhanced methods of CNT synthesis are among the most efficient and precise tools for the production of carbon-based nanostructures, as demonstrated by Keidar⁷ and they have the advantage that the system can operate in a continuous regime. Also, they enable the management of large volumes of carbonaceous materials in solid, liquid or gaseous phase and also allow high power operation.

In addition to CNT, the conversion of methane to hydrogen and CB using the thermal plasma technique has been reported. Among the various methods available, thermal plasma technology has become a viable alternative since the production of CB occurs without the emission of pollutants and the reaction medium is free of oxygen, as proposed by Guo and Kim.⁸ The main reaction that occurs in the pyrolysis of methane by thermal plasma is:



In this study, methane pyrolysis by argon thermal plasma was performed in order to obtain CNT and CB. The CNT were obtained using catalysts coupled to the plasma system and the CB was obtained under the same experimental conditions but without a catalyst.

The technique used to obtain CB and CNT in a thermal plasma system described in this paper has many advantages compared to traditional methods. These include short reaction times (not exceeding 10 min) with methane conversion of up to 90%, and the possibility of obtaining CB and CNT within the same reaction system. Furthermore, according to Fincke *et al.*,⁹ this novel technology using a plasma system for the production of CNT and CB is a clean and environmentally-friendly process with no emissions of CO₂ or similar gaseous pollutants like SO_x or NO_x, producing only solid carbon and hydrogen gas.

Experimental

Pyrolysis experiments

The experimental apparatus used in this study is shown in Figure 1, and the same set up was employed in a previous study by Khalaf *et al.*¹⁰ The DC non-transferred

arc plasma torch consists of a copper cathode (electron emitter) of conical shape and a copper anode in the form of a nozzle or channel. The plasma torch was attached to the top of the reactor or pyrolysis chamber consisting of an iron chamber with an iron liner. Argon (White Martins, 99.5%) was used as the plasma gas and it was introduced into the plasma torch (P) at a controlled flow using a rotameter (R). The electric arc between the cathode and anode (thermal plasma) was initiated by a high voltage discharge generated by a circuit embedded in a continuous power source (F). The methane gas (White Martins, 99.9%) was introduced into the reactor or the pyrolysis chamber (C) from the bottom, and the gaseous products were collected in vials and subjected to gas chromatography analysis. The solid carbon deposited into the liner during the methane degradation was collected directly from the reactor for further analysis.

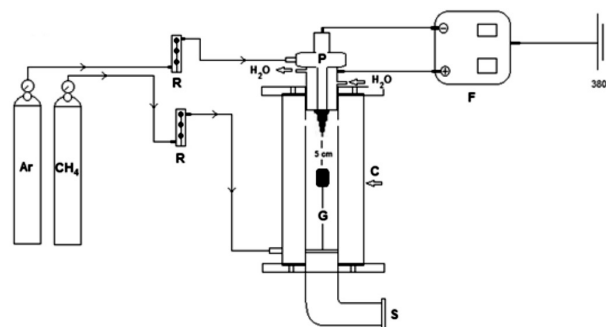


Figure 1. Thermal plasma system: (Ar) argon and (CH₄) methane gas cylinders, (R) rotameters, (P) plasma torch, (F) DC power supply, (C) plasma chamber or reactor, (G) graphite disk, (S) output gases from the pyrolysis.

Table 1 gives a summary of the experimental conditions.

Table 1. Experimental conditions for CNT and CB production

Experimental conditions	
Torch power	6.0 kW
Plasma gas (Ar) flow rate	20 L min ⁻¹
CH ₄ feed rate	5 L min ⁻¹
Run duration	10 min
Temperature (inner wall of the reactor)	700 ± 10 °C

The argon flow rate was fixed at 20 L min⁻¹. The selection of this rate was based on preliminary tests that showed a higher stability of the plasma jet at this value in comparison to other flow rates (5, 10, 15, and 25 L min⁻¹). After the argon had been introduced into the plasma torch, the plasma source was turned on and the DC plasma jet set. At this point, the methane gas was injected immediately

after the thermal equilibrium was reached (which was continuously measured on the inner wall of the reactor and occurred at approximately 700 ± 10 °C). The wall temperature inside the reactor was determined by inserting a type-K thermocouple.

When the tests were performed in the presence of metal catalysts, a graphite disk (G) was inserted into the reactor near the plasma jet (5 cm), and (3 ± 0.002 g) the catalysts (5%Ni/Al₂O₃, 10%Ni/Al₂O₃, and 10%Ni-5%Ce/Al₂O₃) were placed separately on the graphite support. Ni and Ni/Ce catalysts supported on alumina were prepared by wet impregnation according to Nuernberg *et al.*¹¹

In a second step, the carbon samples were characterized using high-resolution scanning electron microscopy (JEOL JSM-6701F, SEM-FEG) coupled with energy dispersive X-ray spectroscopy (EDS), and transmission electron microscopy (JEOL JEM 1200ExII, TEM). The Raman spectra were taken with a Renishaw Raman spectrometer, model inVia, using 514.5 nm argon laser radiation. The specific surface area, pore volume and average pore diameter of the CB samples were determined using a Quantachrome Autosorb-1 instrument. The adsorption/desorption reaction was performed and the data obtained were used to build the N₂ adsorption/desorption curve which in turn allowed the calculation of the surface area, volume and pore width. The specific surface area values were calculated using the method described by Brunauer-Emmett-Teller (BET)¹² and the distributions of the average pore diameter were obtained according to the Barrett-Joyner-Halenda (BJH) method.¹³

Results and Discussion

Characterization of the carbon black

Raman spectroscopy

The Raman spectrum for the carbon product obtained (Figure 2) shows peaks centered in the *D* region of the bands at around 1340 cm^{-1} and its harmonic at around 2800 cm^{-1} along with the *G*-band associated with the tangential stretching at around 1590 cm^{-1} , as proposed by Chu and Li.¹⁴ The profile of this spectrum indicates that the carbon produced during the methane reforming consists of CB as confirmed by the scanning electron microscopy.⁸

Electron microscopy

The study performed using electron microscopy analysis was decisive in the characterization of the sample texture according to the elementary particles and their aggregation state, as well as to characterize the structure of the carbon, for instance, in terms of its crystallinity.⁸

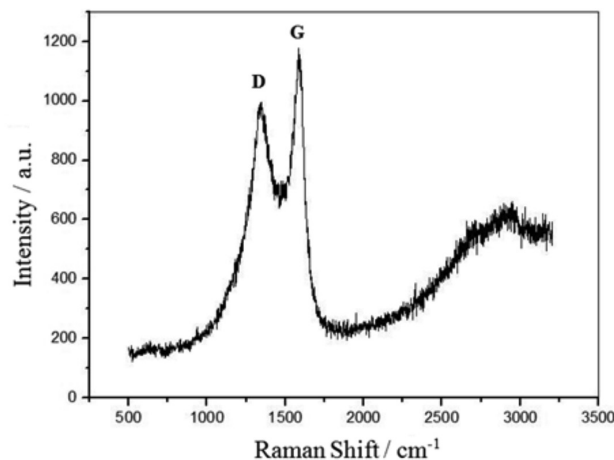


Figure 2. Raman spectrum of the CB sample obtained through the pyrolysis of methane by thermal plasma.

The morphological properties of the carbon obtained during the conversion of methane by thermal plasma were investigated using SEM-FEG (Figure 3A) and TEM (Figure 3B). It can be seen that the samples consist of a large number of randomly-oriented nanoparticles and did not show any structures such as CNT. Figure 3b shows a high magnification image of part of an aggregate where it can be seen that the average diameter of the elementary particles is around 20 nm.

The CB was characterized as presenting a large number of small elementary particles that come together to form aggregates, a characteristic morphology of CB. The aggregates are formed when individual particles stick together through carbon deposition. The structure of the CB formed in the reactor is largely dependent on the formation and concentration of solid particles, as demonstrated by Fulcheri *et al.*⁵

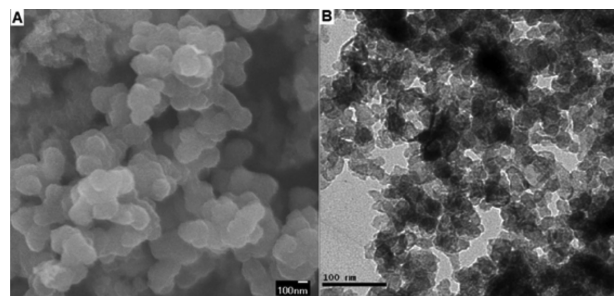


Figure 3. (A) SEM-FEG (15 kV, X 30,000) and (B) TEM (80 kV, X 250,000) images of the CB sample obtained by the pyrolysis of methane via thermal plasma.

Figure 4 shows the results of the chemical analysis of the CB sample using EDS. The sample is composed of 98.79% carbon and 1.21% iron, which comes from the erosion of the reactor caused by the high-temperature plasma jet.

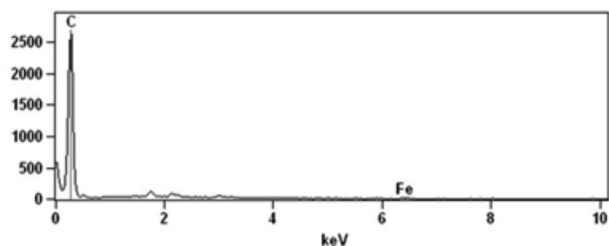


Figure 4. SEM-EDS spectrum of the CB sample obtained from the pyrolysis of methane via thermal plasma.

The effect of temperature on the CB formation using thermal plasma has been studied by other authors. Fulcheri *et al.*⁵ proposed that the temperature of the reaction is of particular importance since it is responsible for the particle size of the CB. According to these authors, 70% yield could be obtained at low reaction temperatures (around 1450 °C), while a yield of 50% of carbon was obtained at temperatures around 1700 °C and the carbon yield decreased at higher temperatures.

Fabry *et al.*¹⁵ showed that although several hypotheses have been proposed to describe the mechanism of carbon particle formation, there is an agreement among scientists in the field that the mechanism involves three distinct phases: (i) nucleation: corresponding to the transformation of a molecular system into a system of particles; (ii) aggregation: due to collisions between nanometer particles (resulting from the nucleation process) to form spherical particles of 10 to 50 nm; and (iii) agglomeration of spherical particles in chains up to around 1 mm in length.

The specific surface area (S_{BET}) of the CB obtained in this study was calculated using the method proposed by Brunauer, Emmett and Teller (BET) and the value obtained was $S_{BET} = 66 \text{ m}^2 \text{ g}^{-1}$. The pore distribution curve based on the BJH method shows that the average pore diameter is approximately 130 nm, indicating a macroporous structure, according to Flory.¹⁶

Carbon nanotubes

Raman spectroscopy

Bystrzejewski *et al.*¹⁷ showed that Raman spectroscopy is a powerful tool to study single-walled carbon nanotubes (SWCNT) and multi-walled carbon nanotubes (MWCNT) via the tangential modes, i.e., *G* band and *D* band. Figure 5 shows the Raman spectra of the CNT samples obtained during the pyrolysis of methane via thermal plasma using different catalysts in the reactor. In all spectra two intense bands were observed at 1333-1353 cm^{-1} and at 1582-1595 cm^{-1} assigned to the *D* and *G* bands (typical for an sp^2 bonded carbon network), respectively, according

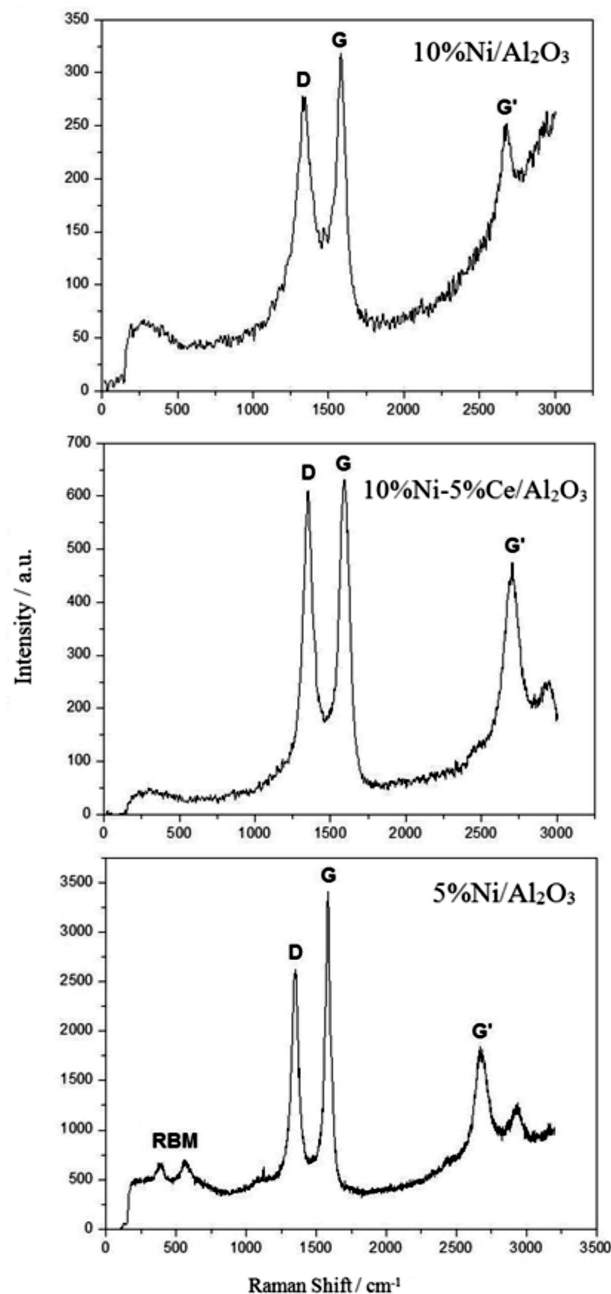


Figure 5. Raman spectra of CNT samples obtained in the presence of different catalysts.

to Numao *et al.*¹⁸ The *D* band is usually related to the presence of amorphous carbon and/or defects in the CNT or impurities and the *G* band indicates ordered carbon structures and/or graphitic carbon.¹⁸ Arepalli *et al.*¹⁹ demonstrated that the *D* band always appears at above 1300 cm^{-1} , and when the width of every *D* band is 30-60 cm^{-1} this characterizes the sample as being comprised of MWCNT. A second-order mode observed between 2450 and 2650 cm^{-1} assigned to the first overtone of the *D* mode is often called *G'* according to Belin and Epron.²⁰ The vibrational breathing modes, called radial breathing

modes (RBM), can be observed at low frequencies on the spectrum (between 100 and 600 cm^{-1}) and are characteristic of SWCNT.²¹ The RBM bands appeared only in the case of the sample obtained with the catalyst 5%Ni/Al₂O₃, which indicates the presence of SWCNT.

Previous studies²²⁻²⁴ considered that the relationship between the intensity of the *D* and *G* bands, given by (I_D/I_G), provides the so-called “quality parameter”, which reflects the proportion of perfect nanotubes in the sample. The presence of perfect and pure CNT structures is more evident when this ratio is close to zero. The values for I_D/I_G obtained in this study are shown in Table 2.

Table 2. The relationship between the intensity of the *D* and *G* bands of different CNT samples

Catalyst	I_D/I_G
10%Ni/Al ₂ O ₃	0.78
10%Ni-5%Ce/Al ₂ O ₃	0.95
5%Ni/Al ₂ O ₃	0.73

The I_D/I_G ratio for all samples indicates the presence of impure or defective CNT, and the sample obtained using the 5%Ni/Al₂O₃ catalyst has the lowest value for the ratio, indicating that this sample contains a higher quantity of pure CNT. This was confirmed by the presence of SWCNT in the sample since these structures have a high degree of graphitization. For the sample obtained using the 10%Ni-5%Ce/Al₂O₃ catalyst the I_D/I_G value was 0.95, which indicates the presence of large amounts of impurities, such as amorphous carbon or defective CNT.

Transmission electron microscopy

The solid carbon formed in the presence of catalysts was characterized by TEM analysis (Figure 6), which provided useful information regarding the morphology of the material.

The TEM images showed that CNT were present in the sample after the plasma reactions had been performed in the presence of the 10%Ni/Al₂O₃ catalyst (Figure 6A). The filaments formed have a high degree of heterogeneity, the tubes being a few microns in length with outside diameters of between 20 and 40 nm. Zhang *et al.*²⁵ demonstrated that the diameter of nanotubes is related to the diameter of the catalyst nanoparticles, indicating that the 10%Ni/Al₂O₃ catalyst is composed of metallic nickel particles of different sizes. The analysis of the carbon samples by TEM also revealed the presence of large amounts of amorphous carbon (the darkest areas on the micrograph). This result verifies that the observed presence of impurities in the CNT sample is in agreement with

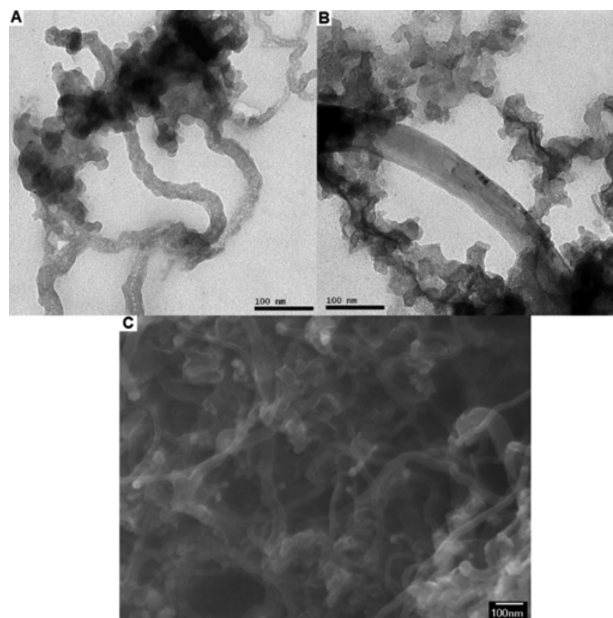


Figure 6. The TEM images obtained after the plasma reaction performed in the presence of the different catalysts: (A) 10%Ni/Al₂O₃; (B) 10%Ni-5%Ce/Al₂O₃; (C) 5%Ni/Al₂O₃.

the Raman spectroscopy analysis. The presence of large amounts of defects in the CNT, such as strictures and sinuous shapes, can also be noted on the micrograph.

The TEM images of the carbonaceous materials obtained using the 10%Ni-5%Ce/Al₂O₃ catalyst (Figure 6B) indicated the growth of CNT. The average diameter of the filaments is 50 nm. It is possible to observe a large amount of amorphous carbon in the sample and even the presence of metallic particles (darker regions) attached to the tubes and inside them.

The tests conducted in the presence of the 5%Ni/Al₂O₃ catalyst (Figure 6C) revealed a large amount of carbon filaments of various diameters, estimated to be between 20 and 100 nm, and a few microns long. This result shows that the 5%Ni/Al₂O₃ catalyst is composed of metallic nickel particles of different sizes, which gives rise to CNT of varying diameter. The nanotubes formed are defective, as shown by the winding shape of the tube (Figure 6C). Applying the same conditions under which the CNT were produced, it was also possible to observe the occurrence of large amounts of amorphous carbon.

In general, the synthesis of CNT in a thermal plasma system occurs in the presence of a metal catalyst.²⁶ Ni is one of the catalyst commonly used in the synthesis of CNT, as demonstrated by Ohishi *et al.*²⁷ Bystrzejewski *et al.*¹⁷ reported the use of Ni and Ce catalysts to synthesize SWCNT by thermal plasma.

The mechanisms involved in CNT carbon vapor nucleation and growth in the presence of a metal catalyst in thermal plasma environments have been previously

investigated. It is known, for example, that the diameter of the CNT is a function of the temperature²⁸ and is almost the same as the diameter of the catalyst.²⁵

Okuno *et al.*²⁹ showed that when the temperature of the reactor walls is 1000-1300 °C, mainly CNT are produced. On the other hand, carbon necklaces are favored when the temperature of the reactor walls is higher (1700-2400 °C). Thus, the temperature distribution inside the plasma reactor is an important factor in relation to the growth of these carbon nanostructures.

As proposed by Okuno *et al.*,²⁹ at 1000-1300 °C the catalytic particles (Figure 7a) are very close to the melting point (the melting temperature of eutectic Ni-C is 1311 °C). Atomic carbons are easily prepared from CH₄, heated and accelerated in the plasma jet.²⁷ According to Okuno *et al.*²⁹ the CNT may form through the diffusion of carbon at the heated particle surface (Figure 7b), which promotes its precipitation into graphene sheets. As the carbon nanotube grows the metal particle is pushed upward (Figure 7c), forming a metal cap which stabilizes the dangling bonds at the edge of the tube by saturating them. The growth of the nanotube stops when the catalytic particle is completely solidified and encapsulated by graphene layers (Figure 7c). A proposed mechanism for the growth of CNT in the presence of metal catalysts (generally transition metals) is shown graphically in Figure 7. A similar mechanism was proposed by Kumar and Ando.³⁰

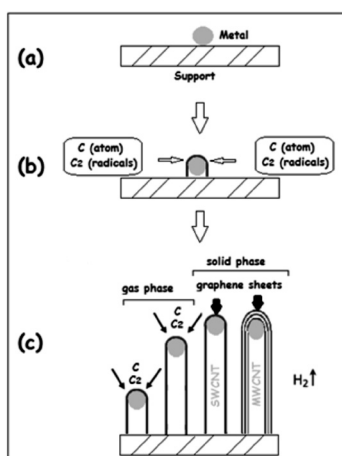


Figure 7. Proposed mechanism for the growth of CNT in the presence of metal catalysts. (a) The metal catalyst and support; (b) C and C₂ generation by thermal plasma followed by carbon diffusion on metal particles and initial CNT nucleation and growth; (c) gas phase CNT growth and solidification of the final products.

The plasma jet provides temperatures which are high enough to decompose CH₄ mainly into C atoms, C₂ radicals and H atoms.⁴ The emission spectrum for C₂ radicals was reported by Bystrzejewski *et al.*,¹⁷ who proposed that the C₂

radicals play a fundamental role in the mechanism involved in the formation of CNT.

The relative quantity of available catalyst particles is a crucial factor in CNT growth and yield. Low quantities will yield by-products such as amorphous carbon, whereas larger quantities will increase the metal-carbon interfaces and yield CNT more efficiently, as shown by Harbec *et al.*³¹ The CNT grown using plasma are still very sensitive to specific condensation conditions like temperature, carbon vapor pressure, particle residence time and also the degree of gas flow turbulence.¹⁷

The synthesis of CNT using the plasma process has the following advantages over other methods: it is possible to achieve higher rates of decomposition of the target hydrocarbons and also higher CNT growth, due to the high temperature and enthalpy of the thermal plasma source. In addition, the plasma power-up can be achieved in a small volume without expansion of the hot plasma zone.⁴

The energy consumption required to convert CH₄ to CB (without a catalyst) or CNT (with a catalyst) was calculated and the value obtained was 0.55 mmol kJ⁻¹. The yield of the reaction was 98% when the CH₄ feed rate was adjusted to 5 L min⁻¹. The theoretical solid carbon yield was 0.24 g of solid carbon in 10 min of plasma treatment. Future work using a plasma reactor with another design will be performed in order to compare the theoretical and experimental yields.

Conclusions

The experiments performed in this study showed the viability of the continuous synthesis of carbon nanostructures of practical interest using a thermal plasma DC system. In this particular synthesis process, CH₄ is directly converted by pyrolysis to solid carbon and hydrogen gas. In the methane pyrolysis experiments that were conducted without the presence of a catalysts in the reactor we observed the formation of amorphous carbon or CB and in the presence of catalysts the analysis showed the formation of CNT.

The thermal plasma DC system employed in this research was not fully optimized and further studies on the production of CNT using this method need to be carried out. However, it can be noted that this method is a promising technique for the large-scale production of CB and CNT because of its numerous advantages including continuous operation and easy scale-up of the plasma power. Further advantages observed include the short reaction time (with each test being performed in under 10 min) and the possibility of obtaining CB and CNT within the same reaction system.

Acknowledgements

The authors are grateful to the Instituto Carbono Brasil and CNPq for the financial support and the INCTcatalysis and LCME-UFSC for help with the analysis.

References

1. Chang, J.-S.; *Sci. Technol. Adv. Mater.* **2001**, *2*, 571.
2. Gomez, E.; Rani, D. A.; Cheeseman, C. R.; Deegan, D.; Wise, M.; Boccaccini, A. R.; *J. Hazard. Mater.* **2009**, *161*, 614.
3. Anderson, T. T.; Dyer, P. L.; Dykes, J. W.; Klavins, P.; Anderson, P. E.; Liu, J. Z.; Shelton, R. N.; *Rev. Sci. Instrum.* **1994**, *65*, 3820.
4. Choi, S. I.; Nam, J. S.; Kim, J. I.; Hwang, T. H.; Seo, J. H.; Hong, S. H.; *Thin Solid Films* **2006**, *506*, 244.
5. Fulcheri, L.; Probst, N.; Flamant, G.; Fabry, F.; Grivei, E.; Bourrat, X.; *Carbon* **2002**, *40*, 169.
6. Harbec, D.; Meunier, J.-L.; Guo, L.; Jureidini, J.; *Carbon* **2007**, *45*, 2054.
7. Keidar, M.; *J. Phys. D: Appl. Phys.* **2007**, *40*, 2388.
8. Guo, X.-F.; Kim, G.-J.; *J. Phys. Chem. Solids* **2008**, *69*, 1224.
9. Fincke, J. R.; Anderson, R. P.; Hyde, T. A.; Detering, B. A.; *Ind. Eng. Chem. Res.* **2002**, *41*, 1425.
10. Khalaf, P. I.; de Souza, I. G.; Carasek, E.; Debacher, N. A.; *Quim. Nova* **2011**, *34*, 1491.
11. Nuernberg, G. B.; Foletto, E. L.; Probst, L. F. D.; Carreño, N. L.V.; Moreira, M. A.; *J. Mol. Catal. A-Chem.* **2013**, *370*, 22.
12. Brunauer, S.; Emmett, P. H.; Teller, E.; *J. Am. Chem. Soc.* **1938**, *60*, 309.
13. Delannay, F.; *Characterization of Heterogeneous Catalysts*, Marcel Dekker: New York, 1984.
14. Chu, P. K.; Li, L.; *Mater. Chem. Phys.* **2006**, *96*, 253.
15. Fabry, F.; Flamant, G.; Fulcheri, L.; *Chem. Eng. Sci.* **2001**, *56*, 2123.
16. Flory, P. J.; *Principles of Polymer Chemistry*, Cornell University Press: New York, 1953.
17. Bystrzejewski, M.; Huczko, A.; Lange, H.; Plotczyk, W. W.; Stankiewicz, R.; Pichler, T.; Gemming, T.; Rümeli, M. H.; *Appl. Phys. A* **2008**, *91*, 223.
18. Numao, S.; Bandow, S.; Iijima, S.; *J. Phys. Chem. C* **2007**, *111*, 4543.
19. Arepalli, S.; Nikolaev, P.; Gorelik, O.; Hadjiev, V. G.; Holmes, W.; Files, B.; Yowell, L.; *Carbon* **2004**, *42*, 1783.
20. Belin, T.; Epron, F.; *Mater. Sci. Eng. B* **2005**, *119*, 105.
21. Chen, B.; Inoue, S.; Ando, Y.; *Diamond Relat. Mater.* **2009**, *18*, 975.
22. Liu, Y.; Pan, C.; Wang, J.; *J. Mater. Sci.* **2004**, *39*, 1091.
23. Enomoto, K.; Kitakata, S.; Yasuhara, T.; Ohtake, N.; Kuzumaki, T.; Mitsuda, Y.; *Appl. Phys. Lett.* **2006**, *88*, 153115.
24. Moreno, J. M. C.; Yoshimura, M.; *J. Am. Chem. Soc.* **2001**, *123*, 741.
25. Zhang, M.; Yudasaka, M.; Iijima, S.; *J. Phys. Chem. B* **2004**, *108*, 12757.
26. Ying, L. S.; Salleh, M. A. b. M.; Yusoff, H. b. M.; Rashid, S. B. A.; Razak, J. b. A.; *J. Ind. Eng. Chem.* **2011**, *17*, 367.
27. Ohishi, T.; Yoshihara, Y.; Fukumasa, O.; *Surf. Coat. Technol.* **2008**, *202*, 5329.
28. Smiljanic, O.; Stansfield, B. L.; Dodelet, J.-P.; Serventi, A.; Désilets, S.; *Chem. Phys. Lett.* **2002**, *356*, 189.
29. Okuno, H.; Grivei, E.; Fabry, F.; Gruenberger, T. M.; Gonzalez-Aguilar, J.; Palnichenko, A.; Fulcheri, L.; Probst, N.; Charlier, J.-C.; *Carbon* **2004**, *42*, 2543.
30. Kumar, M.; Ando, Y.; *J. Nanosci. Nanotechnol.* **2010**, *10*, 3739.
31. Harbec, D.; Meunier, J.-L.; Guo, L.; Gauvin, R.; El Mallah, N.; *J. Phys. D: Appl. Phys.* **2004**, *37*, 2121.

Submitted: May 6, 2013

Published online: November 26, 2013